ENVIRONMENTAL RESEARCH
LETTERS

LETTER • OPEN ACCESS

The response of the ocean carbon cycle to artificial upwelling, ocean iron fertilization and the combination of both

To cite this article: M Jürchott *et al* 2024 *Environ. Res. Lett.* **19** 114088

ENVIRONMENTAL RESEARCH
LETTERS

CrossMark

OPEN ACCESS

RECEIVED
25 July 2024

REVISED
4 October 2024

ACCEPTED FOR PUBLICATION
10 October 2024

PUBLISHED
22 October 2024

LETTER

The response of the ocean carbon cycle to artificial upwelling, ocean iron fertilization and the combination of both

M Jürchott[1,*], **W Koeve**[1] **and A Oschlies**[1,2]

[1] GEOMAR Helmholtz Centre for Ocean Research Kiel, Kiel, Germany
[2] University of Kiel, Kiel, Germany
[*] Author to whom any correspondence should be addressed.

E-mail: mjuerchott@geomar.de

Keywords: carbon dioxide removal (CDR), artificial upwelling (AU), ocean iron fertilization (OIF), biological carbon pump (BCP), export production, iron limitation, oxygen minimum zones

Supplementary material for this article is available online

Abstract

Artificial upwelling (AU) and ocean iron fertilization (OIF) both have been proposed as marine carbon dioxide removal methods to enhance ocean carbon uptake by stimulating the biological carbon pump. We simulate global and regional AU and OIF individually and the combination of both methods between the years 2025 and 2100 in ocean-atmosphere model experiments under the moderate RCP 4.5 CO_2-emission pathway and show that the combination of globally applied AU + OIF yields the greatest ocean carbon uptake potential of +103 Pg C until year 2100. Regional OIF simulated by itself poleward of 45° North and South is responsible for +86.9 Pg C additional ocean carbon uptake. AU-only experiments do not significantly enhance ocean carbon uptake due to the lack of iron in the upwelled waters. We find no consistent relationship between enhanced cumulative export production and changes in the ocean carbon inventory attributable to the biological carbon pump, which makes export production a poor indicator for additional ocean carbon uptake. We identified a strong decrease in the global ocean nitrate inventory (−567 Tmol N) until year 2100 as a consequence of globally applied AU + OIF due to an interrupted balance between N_2-fixation and denitrification.

1. Introduction

The CO_2 concentration in the Earth's atmosphere continuously rises since preindustrial times due to anthropogenic CO_2-emissions, causing an increase in global surface air temperature (IPCC 2022). To limit the global mean surface air temperature increase to well below 2 °C in comparison to preindustrial times, as stated in the Paris Agreement (UNFCCC 2015), we first and foremost need to extensively reduce CO_2 emissions and in addition to this effort, actively remove CO_2 from the atmosphere to compensate future hard-to-abate and potentially also legacy CO_2-emissions (IPCC 2022). Several methods discussed in the scientific literature to actively remove CO_2 from the atmosphere aim to enhance the global ocean's capacity to take up additional CO_2 via marine carbon dioxide removal (mCDR) methods (NASEM 2022).

Two proposed mCDR ideas, artificial upwelling (AU) and ocean iron fertilization (OIF), both aim to supply the surface ocean ecosystem with additional nutrients to stimulate the production and export of organic matter into the ocean interior i.e. the biological carbon pump (BCP) (NASEM 2022). In detail, the OIF-approach describes the idea of releasing bioavailable iron into the surface ocean in high-nutrient-low-chlorophyl (HNLC) ocean regions, in which the ecosystem is limited by iron (Aumont and Bopp 2006, Boyd *et al* 2007, NASEM 2022, Jiang *et al* 2024). Although small-scale field trials of OIF showed a subsequent increase in chlorophyl concentrations after the iron addition, the quantification of additional ocean carbon uptake and carbon storage duration remained challenging (Boyd *et al* 2007). However, Earth system modeling studies show that large-scale OIF around the Southern Ocean

has the potential to significantly enhance ocean carbon uptake via the BCP (Aumont and Bopp 2006, Marinov *et al* 2006, Oschlies *et al* 2010b, Keller *et al* 2014). In contrast to the introduction of additional iron to the surface ocean in the OIF-approach, the AU-approach does not introduce new nutrients to the ocean, but uses vertical ocean pipes to relocate nutrient-rich water from the interior ocean to the sea surface to fertilize the surface ocean ecosystem (Lovelock and Rapley 2007, NASEM 2022). Focusing solely on the nutrient effect of AU, however, recently turned out to be insufficient to estimate the CDR potential of AU, since the CO_2 uptake via AU is strongly dependent on the future CO_2-emission pathway due to stimulated processes associated with the solubility pump (Jürchott *et al* 2023). Furthermore, several Earth-system modeling studies, which found a significant mCDR potential of AU, followed a maximum potential approach for the BCP and/or did not consider iron in the pipe-covered area as a potentially limiting nutrient in the surface layer for net primary production and consequently export production (Yool *et al* 2009, Oschlies *et al* 2010a, Keller *et al* 2014, Jürchott *et al* 2023).

In this study we simulate global and regional AU, OIF and the combination of both methods between the years 2025 and 2100 to investigate complementary or inhibiting effects between both mCDR methods and to better understand the role and the implications of potential iron-limitation for the mCDR-potential of AU. By using two configurations of an Earth System model of intermediate complexity with differences in their representation of the iron cycle under the RCP 4.5 CO_2-emission pathway we specifically investigate and quantify global ocean carbon uptake via AU and OIF individually and in combination, as well as the individual carbon uptake contributions via the BCP and solubility pump, regional differences, ecosystem impacts and side-effects.

2. Methods

2.1. Model configurations

In this study we use two individually calibrated configurations of the UVic 2.9 Earth System model of intermediate complexity (Weaver *et al* 2001, Keller *et al* 2012) with a dynamically coupled energy-balance atmosphere, sea-ice and ocean component (Gent and Mcwilliams 1990, Orr *et al* 1999, Koeve *et al* 2020), which differ in their representation of the marine iron cycle (Keller *et al* 2012, Yao *et al* 2019). In both model configurations all interactions with the biogeochemical land component are intentionally disabled (noLand) in order to isolate the effects of AU and OIF exclusively to the ocean. This procedure has no direct impact on e.g. ocean circulation and allows us to better understand the impact on the marine carbon cycle, but disables potential carbon-concentration and carbon-climate feedbacks from the land model component (Arora *et al* 2020). The three-dimensional ocean component has a spatial resolution of 3.6° longitude and 1.8° latitude and consists of 19 vertical levels ranging from a 50 m thick layer at the surface to up to 500 m thick layers in the deep ocean. The model ocean contains a fully simulated carbon cycle and includes dissolved inorganic carbon (DIC) and alkalinity as prognostic model tracers. The nutrients phosphate and nitrate are calculated as prognostic tracers as well. A marine NPZD-ecosystem model represents the BCP, in which we assume a fixed C–N–P organic matter stoichiometry following Redfield ratio (Keller *et al* 2012), in addition to a simple diagnostic $CaCO_3$ counter pump representation (Schmittner *et al* 2008). Neither primary production nor the production or dissolution of $CaCO_3$ are assumed sensitive to CO_2.

To easily distinguish between both individually calibrated UVic 2.9 model configurations and to ensure continuity with existing literature we refer to them by the names Fe_Mask (Keller *et al* 2012) and Fe_Dyn (Nickelsen *et al* 2015, Yao *et al* 2019). In Fe_Mask iron-limitation is prescribed via a seasonally cycling climatological iron concentration mask at the oceans surface layer taken from the BLING model (Galbraith *et al* 2010). Fe_Dyn contains a data-constrained and calibrated iron cycle with dissolved iron simulated as a prognostic tracer in the model ocean and includes iron-specific processes such as iron scavenging (Tagliabue *et al* 2017) and hydrothermal sources (Yao *et al* 2019). The N–Fe stoichiometry ratio for organic matter in the Fe_Dyn ecosystem model is 1 mol N per 10 μmol Fe and assumed to be constant (Yao *et al* 2019). Since both model versions are individually calibrated, they start from slightly different initial conditions, but their performance for all relevant Earth-system variables during the simulated climate change transient is comparable (figures S1–S3 and S5). We provide a detailed description of both model versions in the supporting information S1.

2.2. Separation of marine carbon pumps

We diagnose the individual impacts on the carbon cycle via the BCP and the solubility pump by introducing two idealized tracers, DIC^{remin} and DIC^{pre}, to the model (Jürchott *et al* 2023). The amount of DIC in the ocean interior exclusively attributable to the BCP is diagnosed via the idealized tracer DIC^{remin}, which is set to zero upon contact with the atmosphere and only increases in the ocean interior via the amount of DIC released into the water column as a consequence of organic matter degradation. The contribution to the ocean DIC inventory exclusively attributable to the solubility pump is diagnosed via the idealized tracer DIC^{pre}, which adopts the total DIC value of the surface layer and preserves it while being transported

to depth through ocean circulation. Both idealized tracers do not influence other model tracers, but are affected by ocean circulation.

2.3. Experimental design

Following individual model spin-up under preindustrial pCO_2 conditions for both model configurations, we simulate the transient period from the year 1765–2005 with historical CO_2-emissions to the atmosphere and continue with the moderate RCP 4.5 CO_2-emission pathway until the year 2100 (Meinshausen *et al* 2011). Historical CO_2-emissions are consistent with historical land-use and fossil fuel CO_2-emissions, but have been individually corrected for the use of our two noLand model configurations to account for the disabled land carbon uptake. This correction is necessary to ensure that both simulations experience the same climate change as their fully coupled counterparts (Koeve *et al* 2020). For details see supporting information S1.

The general design of the simulation of AU is adopted from a previous study conducted with an earlier version of the UVic model (Oschlies *et al* 2010a) and modified as described below. All model tracers and idealized tracers are subject to the upwelling of AU and transferred adiabatically from the grid box at the pipe's source depth to the surface grid box. To ensures volume conservation and compensate the amount of upwelling, we simulate an additional down-welling flux through all intermediate levels. Any redistribution of heat and salinity due to the pipe's activity influences the density structure of the water column and thus, impacts ocean circulation. The source depth of the AU-pipes is kept constant at 500 m (i.e. upper five vertical levels) and the upwelling intensity is set to 0.5 cm d^{-1}. The chosen upwelling intensity translates into the upwelling of a 0.5 cm thick layer per day averaged over the pipe-covered grid boxes. These conditions represent the assumed upper technical feasible limit of AU at the current technological stage (Oschlies *et al* 2010a, Koweek 2022). The effects of OIF are simulated exclusively in Fe_Mask by relaxing any iron-limitation for phytoplankton and diazotrophs at the surface ocean (Keller *et al* 2014). This OIF-implementation ensures, that iron is not limiting ecosystem productivity and is part of the default AU-approach in Keller *et al* (2014) and Jürchott *et al* (2023) in an effort to maximize a BCP response to AU. The AU approach in both studies can therefore be understood as our AU + OIF approach introduced in the next paragraph.

With the Fe_Mask model we carry out three sets of mCDR experiments, in which we simulate AU and OIF individually (Fe_Mask_AU-only, Fe_Mask_OIF-only), as well as both in combination (Fe_Mask_AU + OIF). For the Fe_Dyn model we simulate AU individually (Fe_Dyn_AU-only), since in Fe_Dyn iron is not just represented at the surface ocean but as a prognostic tracer at depth and is therefore subject to the upwelling via AU (see table 1 as well). All four mCDR-simulations are carried out with either (i) a global application area approach, (ii) only in the region equatorward between 45° N and 45° S, or (iii) only in the region poleward of 45° N and 45° S covering high-latitude regions and only where the bathymetry allows for 500 m long vertical pipes (figure S4) (Jürchott *et al* 2024). All three regions, in which we simulate both mCDR approaches individually and in combination, are kept constant over the duration of the experiments.

3. Results & discussion

3.1. Carbon cycle & ecosystem response

Globally simulated AU + OIF yields the greatest ocean carbon uptake of +103 Pg C until year 2100, while global OIF-only is responsible for +95 Pg C (figure 1(a)), which would correspond to avoided emissions of about 124 Pg C (Oschlies *et al* 2010b) and compensate for approximately 27% of the cumulative carbon emissions between year 2025–2100 from the adjusted Fe_Mask noLand RCP 4.5 CO_2 emission pathway (+465 Pg C). We detect neither significant changes in the ocean carbon inventory in both globally simulated AU-only experiments, nor major shifts in the idealized DIC^{remin} and DIC^{pre} tracer contributions (figures 1(b) and (c)). These results suggest, that AU-only is ineffective under the moderate RCP 4.5 CO_2 emission pathway to increase the oceans capacity of additional carbon uptake. Contributing factors, which lead to the ineffectiveness of AU-only to increase ocean carbon uptake, are (i) the low abundance of preformed nutrients at 500 m depth (figure S5), (ii) the constant mCDR application area, which does not allow for variations in the pipe-covered area during model run time to maximize local ocean carbon uptake and avoid outgassing (Oschlies *et al* 2010a, Keller *et al* 2014, Jürchott *et al* 2023), (iii) a constant carbon-to-nutrient stoichiometry in organic matter (Keller *et al* 2012), (iv) the possibility for iron-limitation (see discussion below) and (v) the applied RCP 4.5 CO_2 emission pathway (Jürchott *et al* 2023). Although recent mesocosm studies suggested, that AU might lead to increased C:N ratios compared to Redfield ratio (Baumann *et al* 2021, 2023, Goldenberg *et al* 2022), they contradict with observed and lower C:N ratios in natural upwelling systems, since higher nutrient availability at the surface ocean is generally associated with lower carbon-to-nutrient ratios in biomass (Moreno and Martiny 2018). Our noLand model configurations do not allow for carbon-concentration and carbon-climate feedbacks from the land model component. For OIF-only experiments we expect a negative carbon-concentration feedback, i.e. a carbon flux

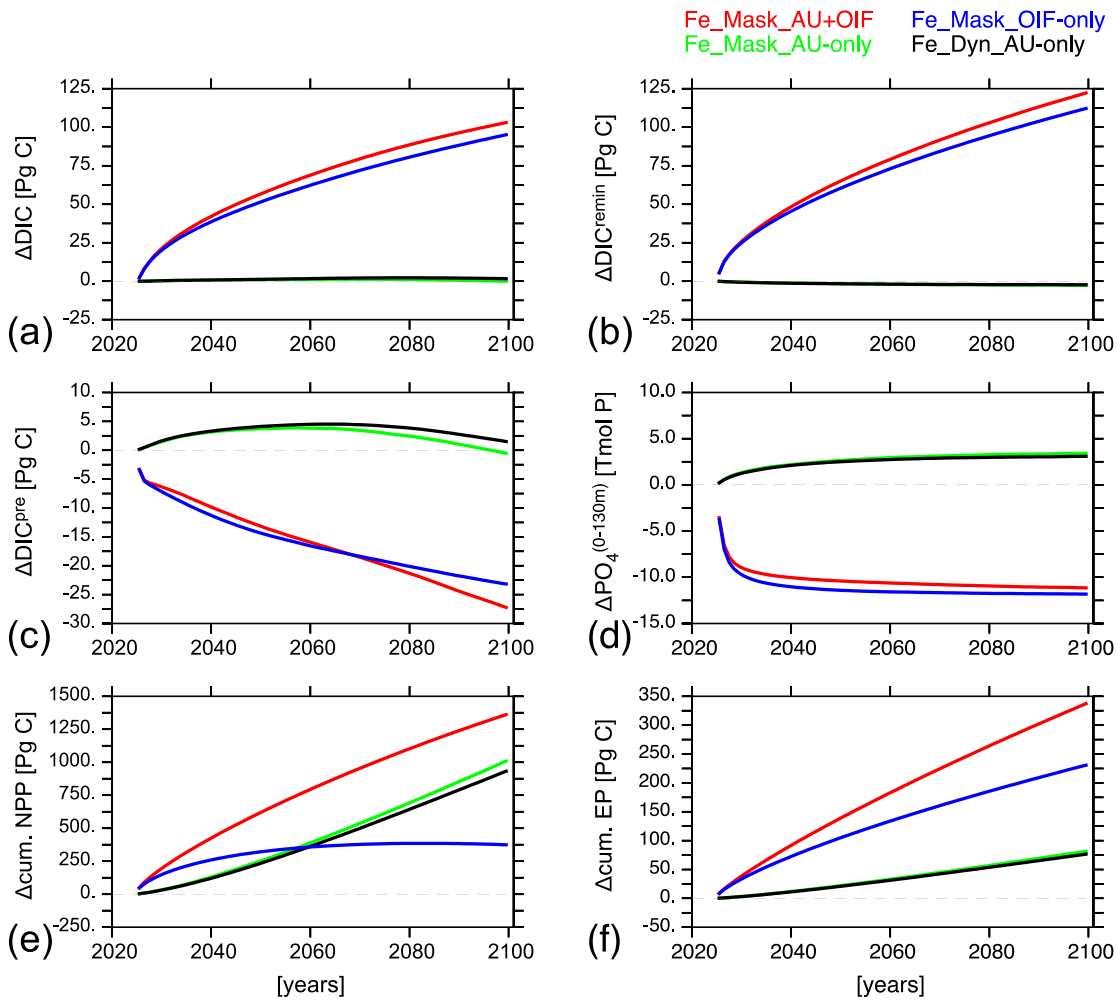

Figure 1. Global changes of marine carbon inventories (a)–(c) and fluxes (e), (f), as well as of surface phosphate inventory (d) from experiments with globally applied artificial upwelling (AU) and ocean iron fertilization (OIF) experiments (see legend) carried out under a moderate CO_2 emission pathway. Changes are quantified from year 2025–2100 and expressed in comparison to the respective reference simulation without CDR. Carbon stocks, ΔDIC (a), ΔDIC^{remin} (b) and ΔDIC^{pre} (c) are in Pg C. ΔPO_4 (d) inventory in the upper 130 m is in Tmol P. Cumulative changes in net primary production (ΔNPP) (e) and export production (ΔEP) (f) are in Pg C. Color code: Fe_Mask_AU + OIF (red), Fe_Mask_OIF-only (blue), Fe_Mask_AU-only (green) and Fe_Dyn_AU-only (black). Green and black line are partly overlapping.

from the land model component into the atmosphere, as a response to reduced atmospheric CO_2 concentrations (e.g. Keller *et al* 2014, 2018). For experiments involving AU, we expect an additional carbon-climate feedback, which would overall increase land carbon uptake as a response to reduced surface air temperatures due to the upwelling of cold water to the surface ocean and subsequent cooling of the atmosphere (Oschlies *et al* 2010a, Keller *et al* 2014).

The combination of globally applied AU + OIF yields a greater mCDR potential than solely anticipated via the individual ocean carbon uptake contributions detected in globally simulated AU-only and OIF-only experiments. The additional ocean carbon uptake in the AU + OIF and the OIF-only experiments is driven by an increase in DIC^{remin} (up to +122 Pg C), i.e. the ocean carbon inventory attributable to the BCP, which is to a minor extent compensated by a decrease in DIC^{pre} (up to −27 Pg C). Note that DIC^{remin} and DIC^{pre} do not entirely add up to the total ocean DIC inventory, since both idealized tracers intentionally do not capture interior ocean DIC changes attributable to the $CaCO_3$ counter pump. Since we apply a fixed carbon-to-nutrient stoichiometry, any increase in DIC^{remin} is a consequence of the utilization of preformed nutrients (Duteil *et al* 2012) by primary producers (Jürchott *et al* 2023). Furthermore, we detect a decrease in the global ocean phosphate inventory in the photic zone in AU + OIF and OIF-only experiments and respective phosphate accumulation in AU-only experiments (figure 1(d)). This accumulation suggests that upwelled phosphate via AU-only cannot be fully utilized by primary producers due to ecosystem limitation via other nutrients (see discussion below).

Our regional experiments reveal that the OIF-only simulation poleward of 45° North and South results in additional ocean carbon uptake of +87 Pg C,

which can explain the bulk effect of the additional ocean carbon uptake detected in the globally simulated OIF-only experiment (table 1). In contrast, AU-only experiments poleward of 45° North and South decrease the ocean carbon inventory by up to −20 Pg C in Fe_Dyn driven by a reduction in DIC^{pre} (−17 Pg C), i.e. changes in the solubility pump. Our mCDR-experiments poleward of 45° North and South cover HNLC regions, in which primary producers are limited by iron (Morel and Price 2003). OIF in such regions does result in the utilization of preformed nutrients and can increase DIC^{remin} independent of a fixed carbon-to-nutrient stoichiometry in the model ecosystem. AU-only experiments equatorward between 45° North and South yield no significant potential for mCDR and the combination of AU + OIF results in greater ocean carbon uptake (+22 Pg C) compared to OIF-only (+16 Pg C). We conclude that OIF is in our experiments the main driver for the increase in the oceans carbon inventory and AU-only experiments do not significantly change or even negatively impact ocean carbon uptake, especially if simulated poleward of 45° North and South.

Under all simulated mCDR approaches, cumulative net primary production and export production increase (figures 1(e) and (f); table 1). However, in the globally applied OIF-only simulation cumulative net primary production increase saturates after year 2060 due to the missing re-supply of interior ocean macronutrients to the surface as provided via AU. This plateau, however, does not limit continuous cumulative export production increase, which is in the OIF-only simulation even higher (+231 Pg C) compared to AU-only simulations (up to +81 Pg C), despite lower cumulative net primary production. We find no consistent relationship between cumulative export production to DIC^{remin}, which could be comprehensively applied to all simulated mCDR experiments and is consistent over time (figures 3(a), S6). Export production and organic matter respiration in the ocean interior, are key processes of ocean carbon uptake via the BCP (Frenger *et al* 2024). While AU-only experiments stimulate export production, they fail to increase DIC^{remin}. The globally applied OIF-only simulation enhances cumulative export production and DIC^{remin} in a ratio of 2.1–1 until the end of the century. In combination with AU, we find a disproportionate additional increase in cumulative export production compared to only a minor increase in DIC^{remin} (2.8–1). Furthermore, our regional experiments reveal for AU + OIF and OIF-only experiments poleward of 45° North and South a cumulative export production to DIC^{remin} ratio again of about 2.1–1 until the end of the century, while the same ratio shifts to 5–1 for AU + OIF and to 2.4 to 1 for OIF only experiments equatorward between 45° North and South. We conclude that a change in export production remains under all simulated mCDR-experiments overall a poor indicator for changes in the ocean carbon inventory attributable to the BCP (Frenger *et al* 2024). This is so despite the fact that our experimental design does not consider potential effects of AU, like changes in particle composition and sinking behavior, which has been observed in experimental work (Baumann *et al* 2021, 2023) and may add to the complexity of carbon export to storage ratio.

3.2. Iron-limitation under AU-only

As stated in the previous section, additional ocean carbon uptake driven via the BCP requires in our model the utilization of preformed nutrients due to the assumption of a fixed carbon-to-nutrient stoichiometry in the model ecosystem. This means for the AU-only experiment performed with the Fe_Dyn UVic configuration, that the amount of phosphate, nitrate and iron prevalent at the surface ocean in addition to the upwelled nutrients via AU must exceed the amount of nutrients required to re-uptake the amount of upwelled DIC^{remin} via primary producers in order to to cause a net increase in DIC^{remin}. A change in the carbon-to-nutrient stoichiometry of organic matter due to AU could further impact additional ocean carbon uptake via the BCP and change the amount of required nutrients to cause a net increase in DIC^{remin}. While an increase in the C:N ratio as suggested by mesocosm experiments might improve the efficiency of the BCP to increase DIC^{remin} (Baumann *et al* 2021, 2023, Goldenberg *et al* 2022), a reduction in the C:N ratio as observed in natural upwelling systems could have the opposite effect (Moreno and Martiny 2018). We find an increase in the global mean surface phosphate and nitrate concentrations and a decrease in the dissolved surface iron concentration in the Fe_Dyn AU-only experiment (figures 2(a), (d), (g)). The lack of dissolved iron at the surface ocean, as also observed in natural HNLC-regions, prevents primary producers to fully utilize the upwelled phosphate and nitrate. As a consequence, the dissolved surface iron concentration limits additional ocean carbon uptake via the BCP. High spatial variation in the change of nutrient concentrations at the surface ocean (figures 2(b), (e), (h)) occurs due to differences in source water nutrient composition (see next paragraph) and the regional response of the ecosystem (figure S7(d)).

To investigate the reason behind the lack of dissolved iron at the surface ocean, we convert all three nutrients at the pipes source depth via their individual carbon-to-nutrient stoichiometry into their DIC-equivalent concentration and divide by DIC^{remin} from the same depth (figures 2(c), (f), (i). A ratio above one indicates an excess of the nutrient in relation to DIC^{remin} and would theoretically promote additional ocean carbon uptake at the surface ocean via the BCP. As shown in figure 2(i), wide regions around the equator and North Pacific are

Table 1. Overview over conducted mCDR-model experiments and changes in Earth-system relevant parameters compared to the respective reference simulation as a consequence of simulated artificial upwelling (AU) + ocean iron fertilization (OIF), AU-only and OIF-only in the UVic 2.9 Fe_Mask model and AU-only simulated in the UVic 2.9 Fe_Dyn model. Each mCDR-approach combination has been applied globally, only equatorward between 45° N and 45° S and only poleward of 45° N and 45° S. Changes in stocks shown for year 2100, changes in cumulative net primary production (NPP) and export production (EP) from year 2025 until 2100 and changes for N_2-fixation and denitrification rates per year for year 2100.

mCDR area	UVic configuration & mCDR-approach	ΔDIC (Pg C)	ΔDIC^{pre} (Pg C)	ΔDIC^{remin} (Pg C)	Δcum. NPP (Pg C)	Δcum. EP (Pg C)	ΔO_2 [Pmol O_2]	ΔNO_3 (Tmol N)	ΔN_2-Fix. (Tmol N yr^{-1})	ΔDenitr. (Tmol N yr^{-1})	ΔSAT (°C)
Global (90°) 345.500.000 (km^2)	Fe_Mask_AU + OIF	103	−27.2	122	1361	337	−15.5	−567	10.3	14.5	−0.45
	Fe_Mask_OIF-only	95.1	−23.2	112	375	231	−14.2	−333	3.23	4.21	−0.28
	Fe_Mask_AU-only	−0.03	−0.53	−2.68	1009	81.4	−0.08	−163	4.86	7.32	−0.15
	Fe_Dyn_AU-only	1.63	1.5	−2.3	932	76.5	−0.08	−206	2.86	6.3	−0.17
Equatorward (45°) 261.900.000 (km^2)	Fe_Mask_AU + OIF	22	−8.56	28.6	870	142	−2.76	−590	11.3	17.1	−0.23
	Fe_Mask_OIF-only	15.6	−4.43	20	−68.6	47.2	−1.77	−310	3.87	5.44	−0.03
	Fe_Mask_AU-only	0.08	−2.78	−0.55	993	78.9	−0.39	−162	4.85	7.29	−0.15
	Fe_Dyn_AU-only	1.26	−1.06	−0.32	910	73.5	−0.42	−205	2.83	6.23	−0.17
Poleward (45°) 90.530.000 (km^2)	Fe_Mask_AU + OIF	84.7	−23.9	101	577	222	−13.5	14.4	−0.35	−1.82	−0.23
	Fe_Mask_OIF-only	86.9	−22	102	524	211	−13.5	16.5	−0.37	−1.79	−0.24
	Fe_Mask_AU-only	−3.54	−0.99	−2.29	24.9	3.93	0.31	−7.01	0.04	0.12	0.02
	Fe_Dyn_AU-only	−19.9	−16.8	−2.66	28.8	3.47	0.42	−14.3	0.07	0.14	0.06

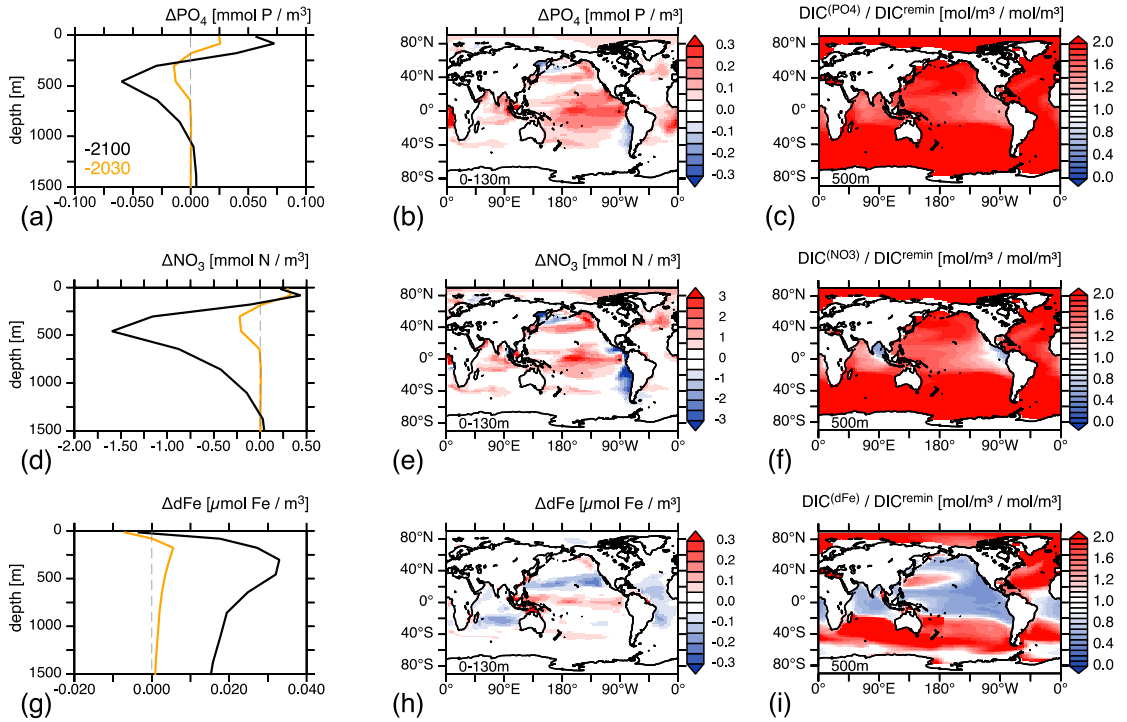

Figure 2. Average nutrient concentration changes due to globally simulated artificial upwelling (AU) in the UVic 2.9 Fe_Dyn model (Fe_Dyn_AU-only). Changes are expressed in comparison to the respective reference simulation without CDR. Left column: change in global average nutrient concentration over depth for ΔPO_4 (a), ΔNO_3 (d) and ΔdFe (g) for year 2030 (orange) and 2100 (black). Middle column: change in spatially resolved average surface nutrient concentration for upper 130 meter of water column for ΔPO_4 (b), ΔNO_3 (e) and ΔdFe (h) for year 2100. Right column: ratio between $DIC^{nutrient}$ to DIC^{remin} at 500 m depth and year 2100 for the AU experiment. Nutrient concentration is converted into its DIC-equivalent via fixed C-nutrient stoichiometry in mol m^{-3} and divided by DIC^{remin} in mol m^{-3} for PO_4 (c), NO_3 (f) and dFe (i). Ratio above (below) one indicates excess (lack) of nutrient in relation to DIC^{remin}.

iron-depleted at 500 m depth in relation to DIC^{remin}, which can explain the average lack of dissolved iron at the surface ocean. Since this pattern is specific to the ratio derived from iron and DIC^{remin} (see figures 2(c) and (f) as well), we argue that it is a consequence of the iron-specific process iron-scavenging (Tagliabue *et al* 2017), which exports iron via sticking itself to the surface of other sinking particles to greater depth compared to DIC, phosphate and nitrate. Overall contributing factors to the pattern at depth shown in figure 2(i) are (i) regional differences in the initial iron input to the surface ocean via the atmosphere and from the seafloor via hydrothermal sources and (ii) the regional activity of the BCP and in extension the regional potential for iron scavenging. In contrast to the previously described pattern, in the Fe_Dyn AU-only experiment poleward of 45° North and South, we find a global inventory decrease in DIC^{remin} (−2.7 Pg C; table 1), despite the upwelling of sufficient dissolved iron in relation to DIC^{remin} around the Southern Ocean. This decrease around the Southern Ocean (see figure S8 as well) cannot be explained by the lack of iron in the upwelled waters, but is probably a consequence of the complex regional circulation patterns around the Southern Ocean (Marinov *et al* 2006), which complicates the regional relationship between upwelled nutrients, export production and DIC^{remin} under AU-only even further.

The increase in the global mean surface phosphate concentration in the AU-only experiment performed with the Fe_Dyn UVic configuration is only possible due to an equal concentration decrease around the pipes source depth, i.e. a redistribution effect (figure 2(a)). As for dissolved iron, we find, except directly at the ocean surface, an increase in the dissolved iron concentration through the entire water column (figure 2(g)). Since atmospheric and hydrothermal iron sources are exactly the same between the reference and the AU-only experiments performed in Fe_Dyn, we argue that the continuous increase in cumulative net primary production, which can be thought of as a living short-term reservoir for iron, and the upwelling activity itself of AU extends the residence time for dissolved iron in the water column, despite enhanced export production and consequently enhanced iron-scavenging. The decrease in the global average nitrate concentration at the pipes' source depth, however, is much greater compared to its increase at the ocean surface (figure 2(d)), which will be discussed in the next section.

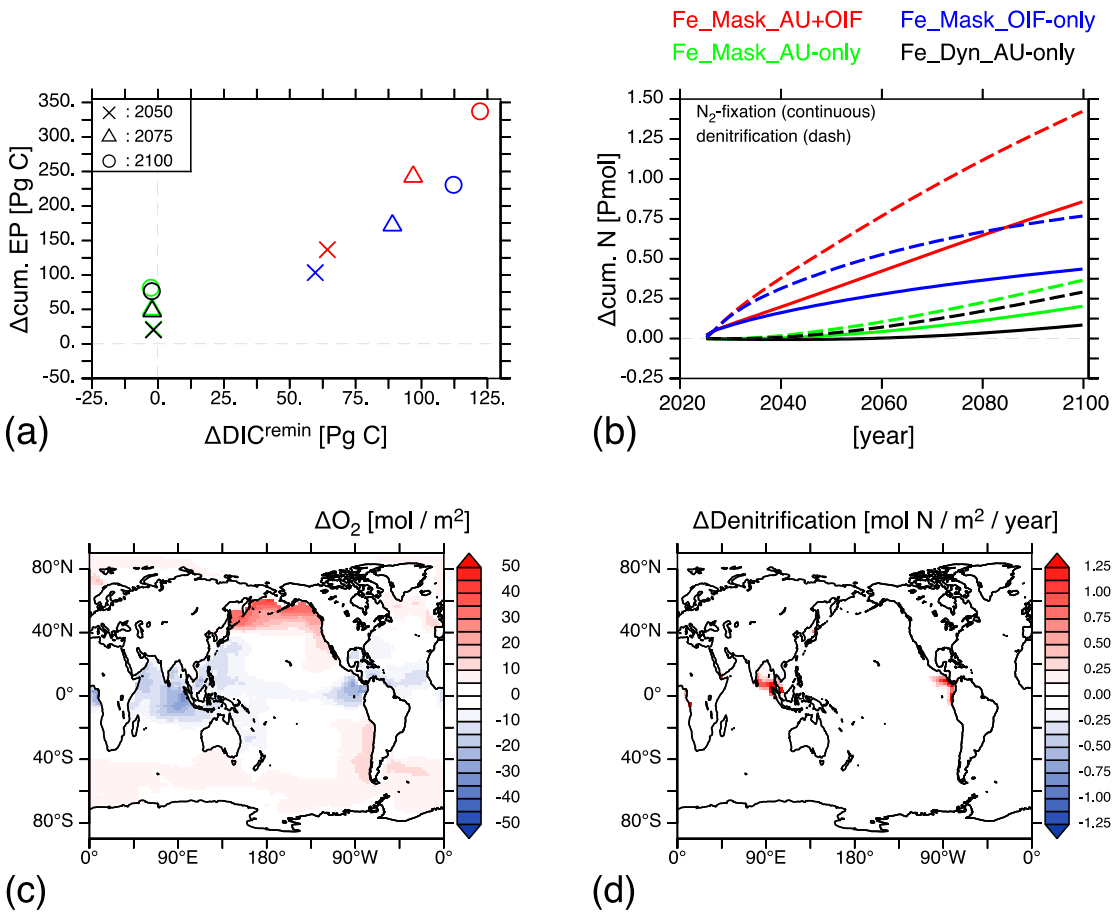

Figure 3. Global changes in variables associated with the biological carbon pump and their impact on the nitrogen cycle. Changes are expressed in comparison to the respective reference simulation without CDR. Relationship between changes in (a) cumulative export production (ΔEP) to ΔDIC^{remin} in Pg C for three timesteps and (b) cumulative changes in global ΔN_2-fixation (continuous lines) and Δdenitrification (dashed lines) in Pmol N. The same color code applies as in figure 1. Spatially resolved and vertically integrated changes for the Fe_Dyn global artificial upwelling (Fe_Dyn _AU-only) experiment for (c) ΔO_2 in mol m^{-2} and (d) Δdenitrification in mol N m^{-2} yr^{-1} for year 2100.

3.3. Out-of-balance nitrogen cycle

We find in all experiments with globally simulated mCDR a decrease in the global ocean nitrate inventory of up to −567 Tmol N until year 2100 for the AU + OIF experiment. In both UVic calibrations ocean nitrate concentrations can increase via N_2-fixation and decrease via denitrification in the absence of oxygen (Keller *et al* 2012). In our reference simulations, both processes are in balance and keep the ocean nitrate inventory stable (figure S3), despite that the global ocean oxygen inventory slowly declines as a response to increased stratification and an overall weakened overturning circulation (Helm *et al* 2011). We detect in all globally simulated mCDR experiments a disproportionately stronger increase in denitrification compared to N_2-fixation (figure 3(b)), which leads to an overall decline in the ocean nitrate inventory (table 1). The increase in denitrification happens in our model simulations via the expansion of naturally existing oxygen minimum zones off the Peruvian and Indian coastlines, which are included in our global and equatorward mCDR application areas (figures 3(c) and (d)). In our model simulations we neither simulate the production of the potent greenhouse gas N_2O, nor its impact on atmospheric temperatures. However, enhanced denitrification as detected in our mCDR experiments could cause the production of additional N_2O and, especially if upwelled via AU directly in contact with the atmosphere, might offset some of the atmospheric carbon reduction effect on atmospheric temperatures (Jin and Gruber 2003, Dutreuil *et al* 2009). We conclude that AU, OIF and the combination of both disrupt the balance between N_2-fixation and denitrification towards a reduced global ocean nitrate inventory via the expansion of oxygen minimum zones and thus, potentially promote conditions for enhanced N_2O production.

4. Conclusions

Our model experiments performed under the moderate RCP 4.5 emission pathway suggest that the combination of globally applied AU + OIF yields the

greatest potential for additional ocean carbon uptake driven via the BCP, while AU-only experiments do not significantly increase the ocean carbon inventory. Further we show that the combination of globally applied AU + OIF yields a greater mCDR potential than solely anticipated via the individual ocean carbon uptake contributions detected in globally simulated AU-only and OIF-only experiments. For AU-only experiments, we identified iron as the limiting nutrient at the surface ocean, which limits the utilization of upwelled preformed phosphate and nitrate via primary producers and prevents additional ocean carbon uptake via the BCP. For OIF-only experiments, the additional ocean carbon uptake is driven via the BCP poleward of 45° North and South covering HNLC-regions.

Net primary production increases under AU and OIF individually and in combination, which has the potential to increase fish-stocks and promote food production (Kirke 2003). The increase in net primary production translates into an increase in export production, but we find no consistent relationship between cumulative export production to DIC^{remin}, which could be comprehensively applied to all simulated mCDR approaches and ocean regions. Thus, a change in export production remains in our model experiments overall a poor indicator for changes in DIC^{remin}, which is a preferred metric for the contribution of biology to the marine carbon sink (Frenger *et al* 2024). However, experimentally simulated changes in mesocosm studies due to AU in the C:N stoichiometry in phytoplankton, as well as the consideration of other nutrients such as silicate and the representation of diatoms and coccolithophores and related possible changes in organic particle sinking speed, carbonate production and ballasting, enhance the complexity of the potential BCP response to AU (Baumann *et al* 2021, 2023, Goldenberg *et al* 2022, 2024, Ortiz *et al* 2022). We emphasize that these specific processes are currently not represented in such great detail in our model experiments, but could further impact and shape the response of the BCP to AU.

In our model experiments we detect an out-of-balance nitrogen cycle as a consequence of a disproportionately stronger increase in denitrification compared to N_2-fixation, which leads to an overall decline in the ocean nitrate inventory. A decline in the global ocean nitrate inventory may have negative long-term consequences for the ecosystem (Oschlies *et al* 2019, Wu *et al* 2023), which could regionally be offset by enhanced nitrate river discharge (Bouwman *et al* 2005, Tivig *et al* 2021). The increase in denitrification is a consequence of expanded oxygen minimum zones particularly in front of the Peruvian and Indian coastlines. Although we do not explicitly simulate N_2O in our model experiments, enhanced denitrification may lead to an increased production of N_2O and, especially if upwelled via AU directly in contact with the atmosphere, might offset any atmospheric carbon reduction effect on atmospheric temperatures (Jin and Gruber 2003, Dutreuil *et al* 2009). We acknowledge limitations of our study related to key model assumptions such as the fixed C:N ratio and propose an AU-MIP with a variety of Earth System models, which e.g. have different vertical resolutions, as a possible way forward to address and reduce uncertainties associated with the mCDR potential of AU.

Data availability statement

The data that support the findings of this study are openly available at the following URL/DOI: https://hdl.handle.net/20.500.12085/56ba983b-169d-4573-96ec-46bd3d925d7e.

Acknowledgment

We acknowledge discussions with colleagues from the Biogeochemical Modelling research unit at GEOMAR. MJ acknowledges funding from German BMBF, Project Test-ArtUp (Grant Number: 03F0897A). This is a contribution to the CDRmare research mission funded by the German Alliance for Marine Research (DAM) and to the Subtopic 6.3 'The future biological carbon pump' of the Helmholtz Earth and Environment research program 'Changing Earth—Sustaining our Future' (POF IV). The author(s) wish to acknowledge discussions with members of the BM-carbon-theme group and the use of the PyFerret program for analysis and graphics in this paper.

ORCID iDs

M Jürchott https://orcid.org/0000-0002-5236-3108
W Koeve https://orcid.org/0000-0002-2298-9230
A Oschlies https://orcid.org/0000-0002-8295-4013

References

Arora V K, Katavouta A, Williams R G, Jones C D, Brovkin V, Friedlingstein P and Ziehn T 2020 Carbon–concentration and carbon–climate feedbacks in CMIP6 models and their comparison to CMIP5 models *Biogeosciences* **17** 4173–222

Aumont O and Bopp L 2006 Globalizing results from ocean in situ iron fertilization studies *Glob. Biogeochem. Cycles* **20** GB2017

Baumann M, Goldenberg S U, Taucher J, Fernandez-Mendez M, Ortiz J, Haussmann J and Riebesell U 2023 Counteracting effects of nutrient composition (Si: n) on export flux under artificial upwelling *Front. Mar. Sci.* **10** 1181351

Baumann M, Taucher J, Paul A J, Heinemann M, Vanharanta M, Bach L T and Riebesell U 2021 Effect of intensity and mode of artificial upwelling on particle flux and carbon export *Front. Mar. Sci.* **8** 742142

Bouwman A F, Van Drecht G, Knoop J M, Beusen A H W and Meinardi C R 2005 Exploring changes in river nitrogen

export to the world's oceans *Glob. Biogeochem. Cycles* **19** GB1002

Boyd P W *et al* 2007 Mesoscale iron enrichment experiments 1993–2005: synthesis and future directions *science* **315** 612–7

Duteil O *et al* 2012 Preformed and regenerated phosphate in ocean general circulation models: can right total concentrations be wrong? *Biogeosciences* **9** 1797–807

Dutreuil S, Bopp L and Tagliabue A 2009 Impact of enhanced vertical mixing on marine biogeochemistry: lessons for geo-engineering and natural variability *Biogeosciences* **6** 901–12

Frenger I, Landolfi A, Kvale K, Somes C J, Oschlies A, Yao W and Koeve W 2024 Misconceptions of the marine biological carbon pump in a changing climate: thinking outside the "export" box *Glob. Change Biol.* **30** e17124

Galbraith E D, Gnanadesikan A, Dunne J P and His-cock M R 2010 Regional impacts of iron-light colimitation in a global biogeochem- ical model *Biogeosciences* **7** 1043–64

Gent P R and Mcwilliams J C 1990 Isopycnal mixing in ocean circulation models *J. Phys. Oceanogr.* **20** 150–5

Goldenberg S U *et al* 2024 Diatom-mediated food web functioning under ocean artificial upwelling *Sci. Rep.* **14** 3955

Goldenberg S U, Taucher J, Fernandez-Mendez M, Ludwig A, Aristegui J, Baumann M, Riebesell U, Stuhr A and Riebesell U 2022 Nutrient composition (Si: n) as driver of plankton communities during artificial upwelling *Front. Mar. Sci.* **9** 1015188

Helm K P, Bindoff N L and Church J A 2011 Observed decreases in oxygen content of the global ocean *Geophys. Res. Lett.* **38** L23602

IPCC 2022 Summary for policymakers *Climate Change 2022: Mitigation of Climate Change. Contribution of Working Group III to the Sixth Assessment Report of the Intergovernmental Panel on Climate Change* ed P R Shukla, J Skea, R Slade, A Al Khourdajie and R van Diemen (Cambridge University Press) (https://doi.org/10.1017/9781009157926.001)

Jiang H B *et al* 2024 Complexities of regulating climate by promoting marine primary production with ocean iron fertilization *Earth Sci. Rev.* **249** 104675

Jin X and Gruber N 2003 Offsetting the radiative benefit of ocean iron fertilization by enhancing N2O emissions *Geophys. Res. Lett.* **30** 2249

Jürchott M, Koeve W and Oschlies A 2024 Supplementary data to Jürchott *et al* (2024): the response of the ocean carbon cycle to artificial upwelling, ocean iron fertilization and the combination of both [dataset] (GEOMAR Helmholtz Centre for Ocean Research Kiel [distributor]) (available at: https://hdl.handle.net/20.500.12085/56ba983b-169d-4573-96ec-46bd3d925d7e)

Jürchott M, Oschlies A and Koeve W 2023 Artificial upwelling—A refined narrative *Geophys. Res. Lett.* **50** e2022GL101870

Keller D P, Feng E Y and Oschlies A 2014 Potential climate engineering effectiveness and side effects during a high carbon dioxide-emission scenario *Nat. Commun.* **5** 1–11

Keller D P, Lenton A, Littleton E W, Oschlies A, Scott V and Vaughan N E 2018 The effects of carbon dioxide removal on the carbon cycle *Curr. Clim. Change Rep.* **4** 250–65

Keller D P, Oschlies A and Eby M 2012 A new marine ecosystem model for the University of Victoria earth system climate model *Geosci. Model. Dev.* **5** 1195–220

Kirke B 2003 Enhancing fish stocks with wave-powered artificial upwelling *Ocean Coast. Manage.* **46** 901–15

Koeve W, Kähler P and Oschlies A 2020 Does export production measure transient changes of the biological carbon pump's feedback to the atmosphere under global warming? *Geophys. Res. Lett.* **47** e2020GL089928

Koweek D A 2022 Expected limits on the potential for carbon dioxide removal from artificial upwelling *Front. Mar. Sci.* **9** 841894

Lovelock J E and Rapley C G 2007 Ocean pipes could help the Earth to cure itself *Nature* **449** 403

Marinov I, Gnanadesikan A, Toggweiler J R and Sarmiento J L 2006 The southern ocean biogeochemical divide *Nature* **441** 964–7

Meinshausen M *et al* 2011 The RCP greenhouse gas concentrations and their extension from 1765 to 2300 *Clim. Change* **109** 213–41

Morel F M and Price N M 2003 The biogeochemical cycles of trace metals in the oceans *Science* **300** 944–7

Moreno A R and Martiny A C 2018 Ecological stoichiometry of ocean plankton *Annu. Rev. Mar. Sci.* **10** 43–69

National Academies of Sciences, Engineering, and Medicine 2022 *A Research Strategy for Ocean-based Carbon Dioxide Removal and Sequestration* (The National Academies Press) (https://doi.org/10.17226/26278)

Nickelsen L, Keller D P and Oschlies A 2015 A dynamic marine iron cycle module coupled to the University of Victoria Earth system model: the Kiel Marine biogeochemical model 2 for UVic 2.9 *Geosci. Model. Dev.* **8** 1357–81

Orr J C, Najjar R, Sabine C L and Joos F 1999 Abiotic-HOWTO, internal OCMIP report, LSCE/CEA Saclay p 25

Ortiz J, Arístegui J, Taucher J and Riebesell U 2022 Artificial upwelling in singular and recurring mode: consequences for net community production and metabolic balance *Front. Mar. Sci.* **8** 743105

Oschlies A, Koeve W, Landolfi A and Kähler P 2019 Loss of fixed nitrogen causes net oxygen gain in a warmer future ocean *Nat. Commun.* **10** 2805

Oschlies A, Koeve W, Rickels W and Rehdanz K 2010b Side effects and accounting aspects of hypothetical large-scale Southern Ocean iron fertilization *Biogeosciences* **7** 4017–35

Oschlies A, Pahlow M, Yool A and Matear R J 2010a Climate engineering by artificial ocean upwelling: Channelling the sorcerer's apprentice *Geophys. Res. Lett.* **37** L04701

Schmittner A, Oschlies A, Matthews H D and Galbraith E D 2008 Future changes in climate, ocean circulation, ecosystems, and biogeochemical cycling simulated for a business-as-usual CO_2 emission scenario until year 4000 AD *Glob. Biogeochem. Cycles* **22** GB1013

Tagliabue A, Bowie A R, Boyd P W, Buck K N, Johnson K S and Saito M A 2017 The integral role of iron in ocean biogeochemistry *Nature* **543** 51–59

Tivig M, Keller D P and Oschlies A 2021 Riverine nitrogen supply to the global ocean and its limited impact on global marine primary production: a feedback study using an Earth system model *Biogeosciences* **18** 5327–50

UNFCC 2015 Adoption of the Paris Agreement FCCC/CP/2015/L.9/Rev.1

Weaver A J *et al* 2001 The UVic earth system climate model: model descrip- tion, climatology, and applications to past, present and future climates *Atmos.-Ocean* **39** 361–428

Wu J, Keller D P and Oschlies A 2023 Carbon dioxide removal via macroalgae open-ocean mariculture and sinking: an Earth system modeling study *Earth Syst. Dyn.* **14** 185–221

Yao W, Kvale K F, Achterberg E, Koeve W and Oschlies A 2019 Hierarchy of calibrated global models reveals improved distributions and fluxes of biogeochemical tracers in models with explicit representation of iron *Environ. Res. Lett.* **14** 114009

Yool A, Shepherd J G, Bryden H L and Oschlies A 2009 Low efficiency of nutrient translocation for enhancing oceanic uptake of carbon dioxide *J. Geophys. Res.* **114** C08009